

# New Conjugated Molecules with Two and Three Dithienyldiketopyrrolopyrrole (DPP) Moieties Substituted at *meta* Positions of Benzene toward p- and n-Type Organic Photovoltaic Materials

Chenmin Yu, Chang He, Yang Yang, Zhengxu Cai, Hwei Luo, Wenqiang Li, Qian Peng, Guanxin Zhang, Zitong Liu,\* and Deqing Zhang\*<sup>[a]</sup>

**Abstract:** Two conjugated molecules, **TADPP3** and **TADPP2-TT**, are reported, in which three and two dithienyldiketopyrrolopyrrole (DPP) moieties, respectively, are substituted at the *meta* positions of benzene. Based on cyclic voltammetry and absorption data, **TADPP3** and **TADPP2-TT** possess similar HOMO and LUMO energies of about  $-5.2$  and  $-3.4$  eV, respectively. Thin films of **TADPP3** and **TADPP2-TT** exhibit p-type semiconducting behavior with hole mobilities of  $2.36 \times 10^{-3}$  and  $3.76 \times 10^{-4} \text{ cm}^2 \text{ V}^{-1} \text{ s}^{-1}$  after

thermal annealing. Molecules **TADPP3** and **TADPP2-TT** were utilized as p-type photovoltaic materials to fabricate organic solar cells after blending with phenyl  $C_{71}$  butyric acid methyl ester (**PC<sub>71</sub>BM**) and phenyl  $C_{61}$  butyric acid methyl ester (**PC<sub>61</sub>BM**). The relatively low  $J_{SC}$  and fill factor values can be attributed to poor film morphologies

**Keywords:** donor–acceptor systems • electrochemistry • fullerenes • organic solar cells

based on AFM and XRD studies. A solar cell with a thin film of **TADPP3** with **PC<sub>71</sub>BM** in a weight ratio of 1:2 exhibits a high open-circuit voltage ( $V_{OC}$ ) of 0.99 V and a power conversion efficiency (PCE) of 2.47%. Interestingly, **TADPP3** can also be employed as an n-type photovoltaic material. The blended thin film of **TADPP3** with **P3HT** in a weight ratio of 1:2 gave a high  $V_{OC}$  of 1.11 V and a PCE of 1.08% after thermal annealing.

## Introduction

Diketopyrrolopyrrole (DPP) is a planar and polar electron-acceptor moiety with strong absorptions in the visible region.<sup>[1,2]</sup> Thus, DPP has been intensively investigated to construct electron donor–acceptor (D-A) molecules and polymers for optoelectronic materials, in particular, for organic photovoltaic materials.<sup>[3–8]</sup> A number of DPP-containing D-A conjugated polymers were reported.<sup>[6–8]</sup> Janssen and co-workers<sup>[7c]</sup> described DPP-containing low band gap polymers with oligothiophene or thienylthieno[3,2-*b*]thiophene as electron donors. These conjugated polymers with relatively high carrier mobilities were successfully utilized as electron donors for organic solar cells (OSCs) with remarkably high power conversion efficiencies (PCEs, above 7%). However, conjugated polymers suffer from broad molecular-weight distributions, end-group contamination, difficult pu-

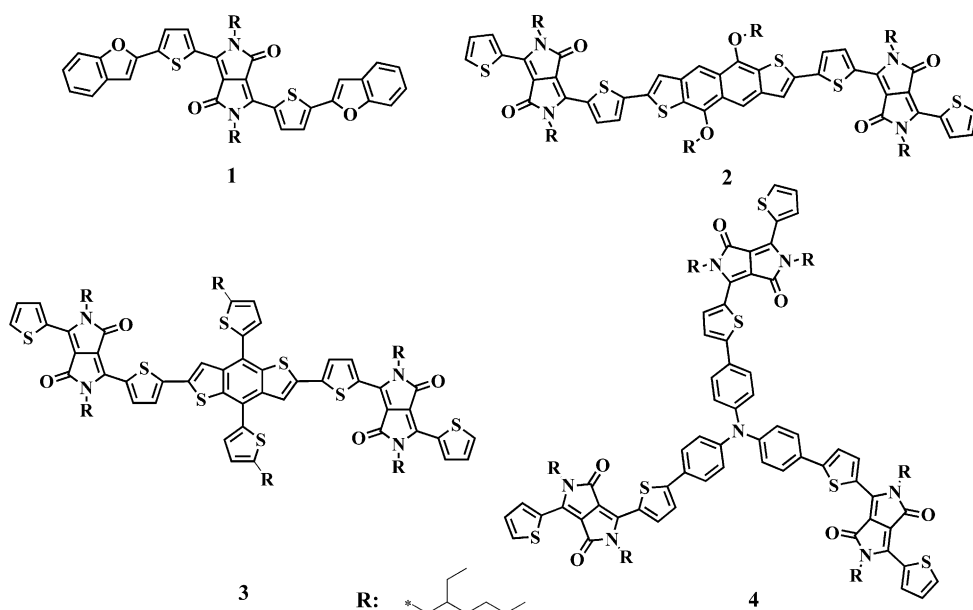
rification methods, and batch-to-batch variations.<sup>[9–14]</sup> These problems can be detrimental for practical applications of conjugated polymers in OSCs.

In comparison, small conjugated molecules possess advantages in terms of ease of synthesis and purification, which can greatly improve the reproducibility of device fabrication.<sup>[9–14]</sup> In addition, small molecules tend to self-assemble into ordered domains and their intermolecular arrangements can be clarified by crystal-structure analysis. In fact, various D-A molecules were investigated for photovoltaic materials.<sup>[15–18]</sup> Nguyen and co-workers reported a series of D-A-D molecules with DPP as the electron-accepting moieties. Solar cells with a blend of thin films of compound **1** (Scheme 1), in which the DPP moiety is flanked with two benzofuran moieties and phenyl  $C_{71}$  butyric acid methyl ester (**PC<sub>71</sub>BM**) exhibited a PCE higher than 4.4%.<sup>[16b]</sup> Marks and co-workers reported A-D-A compound **2**, in which the donor is flanked by DPP moieties, and the combination of **2** (Scheme 1) with phenyl  $C_{61}$  butyric acid methyl ester (**PC<sub>61</sub>BM**) led to solar cells with a PCE of 4.06%.<sup>[16c]</sup> A PCE of 5.29% was achieved with A-D-A compound **3** (Scheme 1) and **PC<sub>71</sub>BM** as the active layer after optimization of the thin-film morphology.<sup>[16e]</sup>

The results demonstrate that small A-D-A and D-A-D molecules are promising for photovoltaic materials of high performance. Nevertheless, small molecules exhibit lower performances compared with the respective conjugated polymers.<sup>[6–8,16–18]</sup> This may be because conjugated polymers

[a] C. Yu, Dr. C. He, Y. Yang, Z. Cai, H. Luo, W. Li, Dr. Q. Peng, Dr. G. Zhang, Dr. Z. Liu, Prof. D. Zhang  
Beijing National Laboratory for Molecular Sciences  
Organic Solids Laboratory, Institute of Chemistry  
Chinese Academy of Sciences  
Beijing 100190 (P.R. China)  
Fax: (+86)10-62562693  
E-mail: drzitong@gmail.com  
dqzhang@iccas.ac.cn

Supporting information for this article is available on the WWW under <http://dx.doi.org/10.1002/asia.201400089>.



Scheme 1. Chemical structures of representative DPP-containing conjugated molecules 1-4.

form thin films and heterojunctions with appropriate electron acceptors more easily. Conjugated molecules with multi-A-D-A or D-A-D moieties may improve the thin-film formation abilities and, at the same time, their chemical structures are definite; moreover, the frontier orbital levels and intermolecular interactions can be finely tuned. Therefore, conjugated molecules with such frameworks have re-

ceived increasing attention for developing new organic photovoltaic materials. Zhan and co-workers described compound **4** (Scheme 1), with three dithienyl-DPP moieties linked to triphenylamine, which was employed as an electron acceptor to fabricate a solar cell with a PCE of 1.2% after blending with poly(3-hexylthiophene-2,5-diyl) (**P3HT**).<sup>[18c]</sup> Herein, we report two conjugated molecules (**TADPP3** and **TADPP2-TT**; Scheme 2) with two and three dithienyl-DPP moieties substituted at the *meta* positions of benzene toward new photovoltaic materials. The molecular design rationale is based on the following considerations: 1) DPP moieties flanked with thiophenes show strong absorptions in the visible region and also relatively high carrier mobilities; 2) the 1,3,5-triethynyl benzene ring as the central core is planar and rigid, and substitutions at the 1,3,5-positions are favorable for intermolecular interactions;<sup>[19]</sup> 3) electron donors, such as 2,2':5',2''-terthiophene in **TADPP2-TT**, can be incorporated to finely tune the HOMO/LUMO levels and intermolecular interactions;<sup>[20]</sup> 4) furthermore, these compounds exhibit 2D structures, which may be beneficial for forming multiple carrier-transporting pathways.<sup>[21]</sup> The results reveal that both **TADPP3** and **TADPP2-TT** can function as electron donors (as a p-type photovoltaic material) and the respective solar cells after blending with **PC<sub>71</sub>BM** exhibit PCEs of 2.47 and 1.11%, respectively, with an open-circuit voltage ( $V_{OC}$ ) higher than 0.90 V. Furthermore, **TADPP3** can also be utilized as an electron acceptor (as a n-type photovoltaic material), and the PCE of the solar cell with thin films **TADPP3** and **P3HT** reaches 1.08% with a high  $V_{OC}$  of 1.11 V after thermal annealing. These results demonstrate that such 2D conjugated frameworks of multiple D-A-D moieties is promising for solution-processed OSCs.

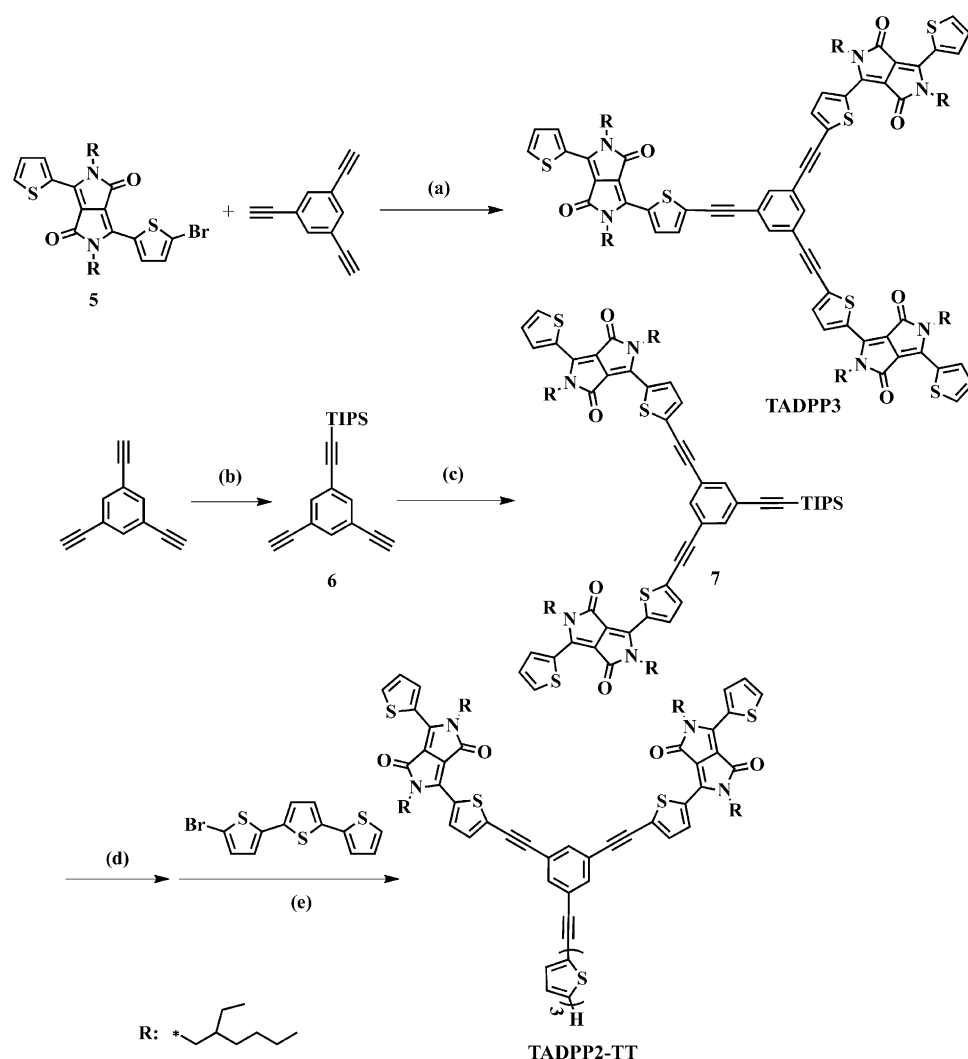
#### Abstract in Chinese:

我们设计并合成了含有两个或三个吡咯并吡咯二酮的星型给受体分子 (**TADPP3** 和 **TADPP2-TT**)。通过电化学和紫外吸收表征, **TADPP3** 和 **TADPP2-TT** 的 LUMO/HOMO 能级分别为 -3.43 eV/-5.24 eV 和 -3.40 eV/-5.23 eV。首先, 我们利用溶液法制备了场效应晶体管器件, **TADPP3** 和 **TADPP2-TT** 均表现为 p 型半导体性质, 其迁移率分别为  $2.36 \times 10^{-3} \text{ cm}^2\text{V}^{-1}\text{s}^{-1}$  和  $3.76 \times 10^{-4} \text{ cm}^2\text{V}^{-1}\text{s}^{-1}$ 。接着我们制备了分别以两者为给体的本体异质结结构太阳能器件, 受体为 **PC61BM** 或 **PC71BM**, 其中当 **TADPP3** 与 **PC71BM** 混合时 (1:2), 其开路电压可高达 0.99V, 且光电转换效率为 2.47%。此外, **TADPP3** 也可作为受体材料, 当其与 **P3HT** 以 1:2 的比例混合时, 其开路电压可高达 1.11V, 且光电转换效率为 1.08%。同时, 我们还利用 XRD 和 AFM 分别表征了它们的场效应和太阳能电池器件的薄膜形貌。

## Results and Discussion

### Synthesis, Characterization, and HOMO/LUMO Energies

The synthesis of **TADPP3** starts from **5** (Scheme 2), which was prepared according to the reported procedure.<sup>[16c]</sup> As shown in Scheme 2, the Sonogashira coupling of **5** with 1,3,5-triethynylbenzene gave **TADPP3** in 72% yield. Compound **TADPP2-TT** was synthesized in three steps. First, 1,3,5-triethynylbenzene was allowed to react with *n*BuLi at  $-78^\circ\text{C}$ , followed by the addition of TIPSCl, leading to **6** in 85% yield. Then, the Sonogashira coupling of **6** with **5** gave



Scheme 2. Chemical structures of **TADPP3** and **TADPP2-TT** and their synthetic routes. Reagents and conditions: a)  $[\text{Pd}(\text{PPh}_3)_4]$ , CuI, diisopropylamine, toluene, 90°C, 72%; b) *n*BuLi, triisopropylsilyl chloride (TIPSCl), -78°C, 85%; c) **5**,  $[\text{Pd}(\text{PPh}_3)_4]$ , CuI, diisopropylamine, toluene, 90°C, 75%; d)  $\text{K}_2\text{CO}_3$ , tetrahydrofuran (THF); e) 5-bromo-2,2':5',2''-terthiophene,  $[\text{Pd}(\text{PPh}_3)_4]$ , CuI, diisopropylamine, reflux, 67%.

**7** in 75% yield. Finally, **TADPP2-TT** was obtained by removal of TIPS in **7** in the presence of  $\text{K}_2\text{CO}_3$ , followed by Sonogashira coupling with 5-bromo-2,2':5',2''-terthiophene. The chemical structures of both compounds were characterized by NMR spectroscopy and MS data and their purities were confirmed with elemental analysis. Both compounds

are thermally stable under 300°C based on the thermogravimetric analysis (TGA) data shown in Figure S1 a in the Supporting Information. The differential scanning calorimetry (DSC) traces of both **TADPP3** and **TADPP2-TT** display no clear phase transition below 250°C (see Figure S1 b and c in the Supporting Information).

Figure 1 shows the cyclic voltammograms of **TADPP3** and **TADPP2-TT**. Three reversible oxidation waves and one reduction wave were observed for **TADPP3**. Similarly, **TADPP2-TT** also displays three reversible oxidation waves and one reversible reduction wave. Based on the respective onset oxidation and reduction potentials of the two compounds, their HOMO and LUMO energies, as well as band gaps, were estimated based on the following equations:

$$\begin{aligned} \text{LUMO} &= -(4.41 + E_{\text{red1}}^{\text{onset}}) \text{ eV}, \text{ HOMO} = \\ &= -(E_{\text{ox1}}^{\text{onset}} + 4.41) \text{ eV} \quad (\text{see Table 1}). \end{aligned}$$

Interestingly, both compounds possess similar HOMO (ca. -5.2 eV) and LUMO (ca. -3.4 eV) energies. This is indeed in agreement with the absorption data and theoretical calculation results (see below). Figure 1 also shows the respective HOMO and LUMO levels of **TADPP3**, **TADPP2-TT**, **P3HT**, **PC<sub>61</sub>BM**,

and **PC<sub>71</sub>BM**. Notably, the respective LUMO and HOMO energy differences between both **TADPP3/TADPP2-TT** and **P3HT/PC<sub>71</sub>BM (PC<sub>61</sub>BM)** are large enough to guarantee efficient exciton dissociation. Judging from the energy levels, both compounds are suitable as either electron donors or acceptors in OSCs.<sup>[20a]</sup> Moreover, the energy differences be-

Table 1. Absorption and electrochemical data, HOMO/LUMO energies, and band gaps of **TADPP3** and **TADPP2-TT**.

	$\lambda_{\text{max}}/\text{solution}$ [nm] <sup>[a]</sup>	$\lambda_{\text{max}}/\text{film}$ [nm]	$E_{\text{ox1}}^{\text{onset}}$ [V] <sup>[c]</sup>	$E_{\text{red1}}^{\text{onset}}$ [V] <sup>[c]</sup>	LUMO [eV] Exptl <sup>[d]</sup> (Calcd) <sup>[e]</sup>	HOMO [eV] Exptl <sup>[d]</sup> (Calcd) <sup>[e]</sup>	$E_g$ [eV]
<b>TADPP3</b>	584 (102000) <sup>[b]</sup> 547, 376	613, 564, 402, 376	0.83	-0.98	-3.43 (-2.71)	-5.24 (-4.91)	1.81 <sup>[f]</sup> (1.83) <sup>[g]</sup>
<b>TADPP2-TT</b>	583 (55000) <sup>[b]</sup> 545, 385	614, 564, 401, 385	0.82	-1.01	-3.40 (-2.67)	-5.23 (-4.88)	1.83 <sup>[f]</sup> (1.85) <sup>[g]</sup>

[a] Measured in  $\text{CHCl}_3$  ( $1.0 \times 10^{-5}$  M). [b] Molar extinction coefficient ( $\epsilon_{\text{max}}$ ,  $\text{cm}^2 \text{M}^{-1}$ ). [c] In  $\text{CH}_2\text{Cl}_2$  containing  $\text{Bu}_4\text{NPF}_6$  (0.1 M) at a scan rate of  $50 \text{ mV s}^{-1}$ . [d] Estimated from the following equations:  $\text{LUMO} = -(4.41 + E_{\text{red1}}^{\text{onset}})$  eV,  $\text{HOMO} = -(E_{\text{ox1}}^{\text{onset}} + 4.41)$  eV. [e] Based on DFT calculations. [f] Based on redox potentials. [g] Based on absorption spectra data.

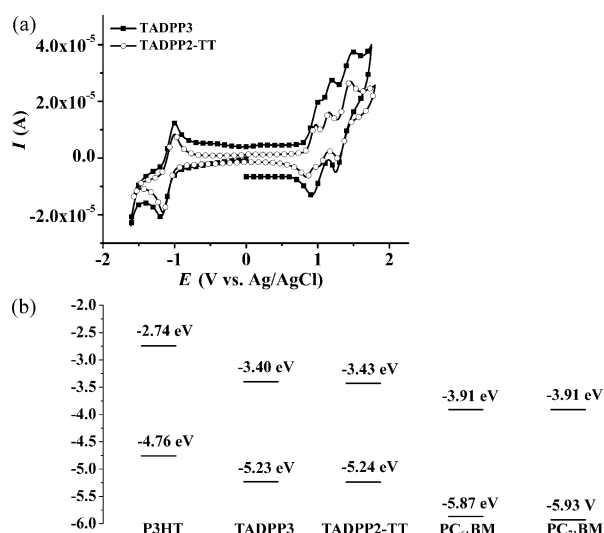


Figure 1. a) Cyclic voltammograms of **TADPP3** and **TADPP2-TT** ( $1.0 \times 10^{-3}$  M) in  $\text{CH}_2\text{Cl}_2$  at a scan rate of  $50 \text{ mV s}^{-1}$ , with platinum as the working and counter electrodes, an Ag/AgCl electrode (saturated KCl) as the reference electrode, and  $n\text{Bu}_4\text{NPF}_6$  (0.1 M) as the supporting electrolyte. b) HOMO/LUMO energy levels of different conjugated molecules and polymers.

tween the HOMO levels of the respective donors and the LUMO levels of the respective acceptors are higher than 1.3 eV; thus high  $V_{\text{OC}}$  values are expected for solar cells with **TADPP3** or **TADPP2-TT** as donors or acceptors after being combined with **PC<sub>71</sub>BM** (**PC<sub>61</sub>BM**) or **P3HT** as the acceptor or donor.

Figure 2 shows the absorption spectra of solutions and thin films of **TADPP3** and **TADPP2-TT**. The solution of **TADPP3** exhibits three broad absorptions at around  $\lambda = 376$

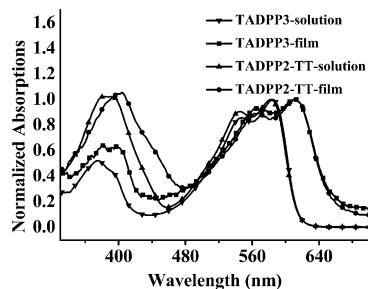


Figure 2. Normalized UV/Vis absorption spectra of **TADPP3** and **TADPP2-TT** in  $\text{CHCl}_3$  ( $1.0 \times 10^{-5}$  M) and their thin films.

( $\epsilon_{\text{max}} = 53000$ ), 547 (87000), and 584 nm ( $102000 \text{ cm}^2 \text{ M}^{-1}$ ). A solution of **TADPP2-TT** also shows strong absorptions in this region at around 385 ( $\epsilon_{\text{max}} = 57000$ ), 545 (50000), and  $\lambda = 583$  nm ( $55000 \text{ cm}^2 \text{ M}^{-1}$ ). It is clear that **TADPP3** shows stronger absorptions above  $\lambda = 440$  nm than those of **TADPP2-TT** based on the molar absorption coefficients. Thus, it is expected that **TADPP3** will show better photovoltaic performance than that of **TADPP2-TT** (see below). Compared with those in solution, the absorption spectra of

thin films of **TADPP3** and **TADPP2-TT** are redshifted. Both thin films of **TADPP3** and **TADPP2-TT** show strong absorptions at  $\lambda \approx 610$  nm, which are extended to  $\lambda = 670$  nm. As a result, they possess rather similar optical band gaps (ca. 1.8 eV) based on the respective onset absorptions. This is in agreement with the band gaps based on cyclic voltammetric data (see Table 1). However, **TADPP2-TT** shows stronger absorption at  $\lambda \approx 380$  nm than that of **TADPP3**. This is probably owing to the presence of the 2,2':5',2''-terthiophene moiety in **TADPP2-TT**. By considering that **P3HT** and **PC<sub>71</sub>BM** absorb strongly in the region of  $\lambda = 400$ –600 and 200–350 nm, respectively, blend films of either **TADPP3** or **TADPP2-TT** with **P3HT** or **PC<sub>71</sub>BM** are expected to absorb strongly in the region of  $\lambda = 300$ –750 nm.

The chemical structures of **TADPP3** and **TADPP2-TT** were investigated with calculations based on DFT. The alkyl chains were replaced by methyl groups. As depicted in Figure 3, the HOMO and LUMO orbitals of **TADPP3** are

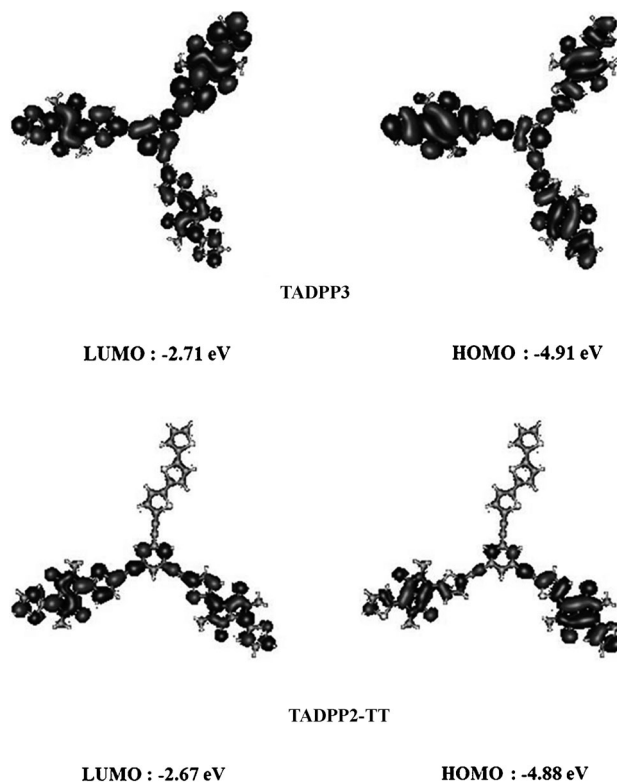


Figure 3. LUMO and HOMO orbitals of **TADPP3** and **TADPP2-TT** obtained by DFT calculations; the alkyl chains were replaced with methyl groups.

delocalized over the three dithienyl-DPP moieties and the central 1,3,5-triethynylbenzene core. For **TADPP2-TT**, HOMO and LUMO orbitals are mainly localized on two DPP moieties; however, the central core contributes slightly to the HOMO/LUMO orbitals, and the 2,2':5',2''-terthiophene moiety makes no contribution to either the HOMO or LUMO orbitals. The calculated HOMO/LUMO energies of **TADPP3** are close to those of **TADPP2-TT** (see

Table 1). These results reveal that the interaction between 2,2':5',2''-terthiophene and the dithienyl-DPP moieties in **TADPP2-TT** are negligible; this is probably because 2,2':5',2''-terthiophene is not fully conjugated with the central benzene core. This agrees well with the observations based on absorption and cyclic voltammetry data (see Table 1). The solvent effects were not included in the theoretical calculations, and thus, the calculated HOMO/LUMO energies of **TADPP3** and **TADPP2-TT** are different from those obtained based on absorption and electrochemical data.

### Thin-Film Organic Field-Effect Transistors (OFETs)

To ensure effective charge-carrier transport to the electrodes and reduce photocurrent loss, high mobility is a basic requirement for photovoltaic materials. To estimate the charge mobilities of thin films of **TADPP3** and **TADPP2-TT**, the respective bottom-gate/bottom-contact organic field-effect transistors (OFETs) were fabricated with conventional techniques (see the Experimental Section). Based on the transfer and output characteristics shown in Figure 4, thin

Table 2. OFET performance data for thin films of **TADPP3** and **TADPP2-TT**.

	$T$ [°C]	$\mu_h$ [ $\text{cm}^2\text{V}^{-1}\text{s}^{-1}$ ] <sup>[a]</sup>	$I_{\text{on/off}}$	$V_{\text{th}}$ [V]
<b>TADPP3</b>	80	$(2.18/1.53) \times 10^{-3}$	$10^6$	-10 to -5
	100	$(2.36/2.06) \times 10^{-3}$	$10^6$	-35 to -15
	120	$(2.07/1.96) \times 10^{-3}$	$10^6$	-40 to -10
<b>TADPP2-TT</b>	80	$(1.24/1.00) \times 10^{-4}$	$10^4$	-22 to -8
	100	$(3.76/2.49) \times 10^{-4}$	$10^4$	-17 to -11
	120	$(2.00/1.88) \times 10^{-4}$	$10^4$	-15 to -5

[a] The mobilities are provided in "highest/average" form; the performance data were obtained based on more than 10 different OFETs.

vacuum. However, the hole mobility starts to decrease after further increasing the annealing temperature (see Table 2). The hole mobility of the as-prepared thin film of **TADPP2-TT** was estimated to be  $1.24 \times 10^{-4} \text{ cm}^2\text{V}^{-1}\text{s}^{-1}$ . Similarly, the hole mobility increases after thermal annealing at 100 °C. It is clear that hole mobilities of thin films of **TADPP3** are higher than those of **TADPP2-TT** (see Table 2). Moreover, the hole mobilities of neither **TADPP3** nor **TADPP2-TT** are significantly affected by thermal annealing. As discussed below, relatively low hole mobilities can be attributed to the low crystallinity and poor morphology of thin films of **TADPP3** and **TADPP2-TT**.

Out-of-plane XRD patterns of thin films of **TADPP3** and **TADPP2-TT** were measured after annealing at different temperatures. As depicted in Figure S2 in the Supporting Information, only broad and weak diffraction peaks at around  $22^\circ$  were detected for a thin film of **TADPP3** after annealing at 100 and 120 °C. Similarly, no sharp diffraction peaks were also observed for a thin film of **TADPP2-TT**. Thus, thin films of both **TADPP3** and **TADPP2-TT** show poor crystallinity, even after thermal annealing. Figures S3 and S4 in the Supporting Information show AFM images of thin films of **TADPP3** and **TADPP2-TT** on octadecyltrichlorosilane (OTS)-modified  $\text{SiO}_2$  substrates after annealing at different temperatures. For a thin film of **TADPP3**, the heights and sizes of molecular domains increase after thermal annealing, but most of these molecular domains are not interconnected. Morphological modifications are rather minor after thermal annealing for the thin film of **TADPP2-TT** (see Figure S4 in the Supporting Information). These results agree well with the fact that thin films of **TADPP3** and **TADPP2-TT** display low carrier mobilities.

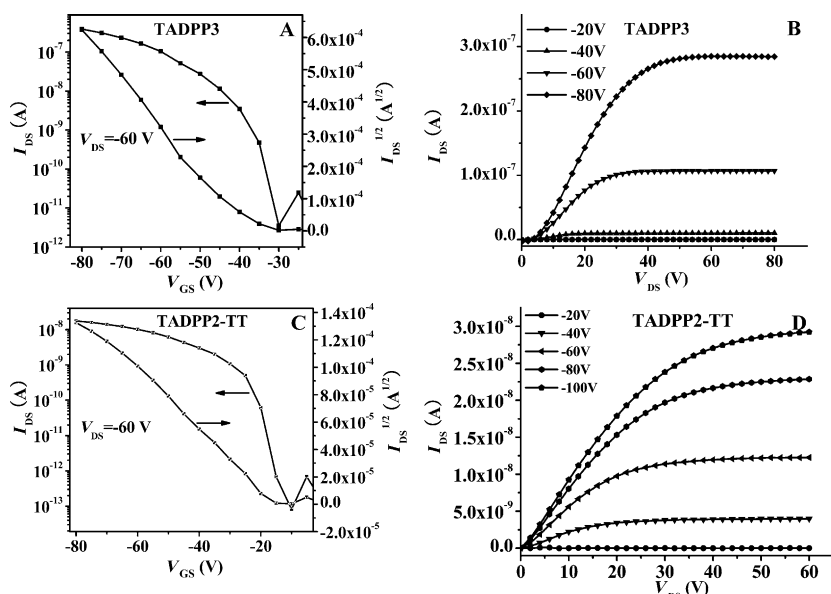


Figure 4. The transfer and output characteristics of OFETs with thin films of **TADPP3** (A and B) and **TADPP2-TT** (C and D) after annealing at 100 °C. The transistor channel width and channel length are 1400 and 50  $\mu\text{m}$ , respectively.

films of both **TADPP3** and **TADPP2-TT** display p-type semiconducting properties. The as-prepared OFET with a thin film of **TADPP3** shows a hole mobility of  $2.18 \times 10^{-3} \text{ cm}^2\text{V}^{-1}\text{s}^{-1}$ , which slightly increases to  $2.36 \times 10^{-3} \text{ cm}^2\text{V}^{-1}\text{s}^{-1}$  after thermal annealing at 100 °C for 1.0 h in

### Photovoltaic Device Performance

By considering their HOMO/LUMO energies, **TADPP3** and **TADPP2-TT** may function as p- and n-type organic photovoltaic materials. First, **TADPP3** and **TADPP2-TT** were examined as p-type organic photovoltaic materials. OSCs were fabricated with the structure indium tin oxide (ITO)/poly(3,4-ethylenedioxythiophene)-poly(styrenesulfonate) (PEDOT:PSS)/donor:**PC<sub>71</sub>PM** (**PC<sub>61</sub>BM**)/LiF/Al, in which **PC<sub>71</sub>PM** and **PC<sub>61</sub>BM** were utilized as electron acceptors. The blend thin films of **TADPP3** or **TADPP2-TT** with either **PC<sub>71</sub>PM** or **PC<sub>61</sub>BM** show strong absorptions in the visible region. For instance, the thin film of **TADPP3** with **PC<sub>71</sub>BM** absorbs from  $\lambda=330$  to 680 nm with an absorption maximum at  $\lambda \approx 554$  nm, whereas that of **TADPP2-TT** with **PC<sub>71</sub>BM** exhibits absorptions in the region of  $\lambda=340$ –660 nm with absorption maxima at  $\lambda \approx 380$  and 555 nm, as shown in Figure S5 in the Supporting Information.

OSCs with blending films of **TADPP3** and **PC<sub>61</sub>BM** in different weight ratios were examined. As listed in Table 3,

Table 3. Photovoltaic performances with **TADPP3/TADPP2-TT** after blending with either **PC<sub>61</sub>PM/PC<sub>71</sub>BM** or **P3HT**.

Donor/acceptor	Ratio (w/w)	$V_{OC}$ [V]	$J_{SC}$ [ $\text{mA cm}^{-2}$ ]	FF [%]	PCE [%]
<b>TADPP3/PC<sub>61</sub>BM</b>	1:1 <sup>[a]</sup>	0.92	2.54	29.1	0.68
	1:2 <sup>[a]</sup>	0.87	3.17	34.1	0.94
	1:3 <sup>[a]</sup>	0.78	3.22	34.1	0.86
<b>TADPP3/PC<sub>71</sub>BM</b>	1:2 <sup>[a]</sup>	0.99	6.24	40.0	2.47
<b>TADPP2-TT/PC<sub>71</sub>BM</b>	1:2 <sup>[a]</sup>	0.97	3.88	30.0	1.11
<b>P3HT/TADPP3</b>	1:1 <sup>[a]</sup>	1.03	1.21	37.3	0.47
	1:1 <sup>[b]</sup>	1.10	1.97	40.3	0.87
	1:2 <sup>[b]</sup>	1.05	0.98	36.8	0.38
	2:1 <sup>[b]</sup>	1.11	2.72	35.7	1.08

[a] As a casted thin film. [b] As a thin film after annealing at 150 °C.

these OSCs exhibit relatively high  $V_{OC}$  up to 0.92 V, but the values of  $J_{SC}$  and fill factor (FF) are low, and thus, PCE values are lower than 1.0% for thin films of **TADPP3** with **PC<sub>61</sub>BM** in different weight ratios. The thin film of **TADPP3** and **PC<sub>61</sub>BM** in a ratio of 1:2 (w/w) yields a PCE of 0.94%. Apart from **PC<sub>61</sub>BM**, **PC<sub>71</sub>BM** was also employed as an electron acceptor to be blended with either **TADPP3** or **TADPP2-TT** for OSCs. Figure 5 shows the respective  $J$ - $V$  curves and incident photon-to-current conversion efficiency (IPCE) spectra for solar cells with **TADPP3** or **TADPP2-TT** after blending with **PC<sub>71</sub>BM**. The results reveal that the blending of thin films of **TADPP3** or **TADPP2-TT** with **PC<sub>71</sub>BM** in a ratio of 1:2 (w/w) lead to better photovoltaic performances. For instance, the PCE increases to 2.47% for the solar cell with **TADPP3** as the active layer; the  $V_{OC}$  is up to 0.99 V after optimization of both ratios and thin-film thicknesses (Table 3 and Table S3 in the Supporting Information). The reduction of thin-film thickness is beneficial for transporting charges to electrodes, and thus, the PCE is enhanced. The combination of **TADPP2-TT** with **PC<sub>71</sub>BM** in a ratio of 1:2 (w/w) yields

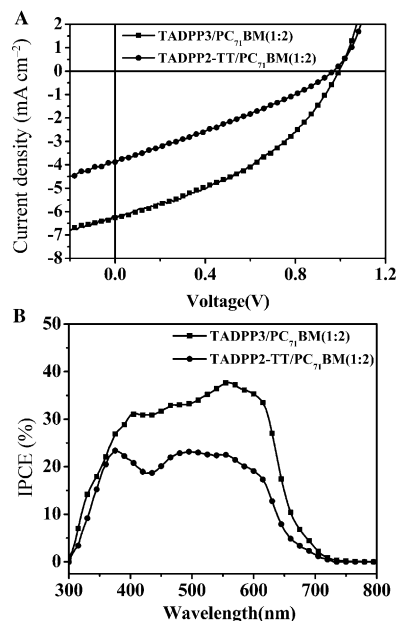


Figure 5. A)  $J$ - $V$  curves and B) IPCE spectra of OSCs with the respective blended thin films of **TADPP3/TADPP2-TT** and **PC<sub>71</sub>BM**; the weight ratios are indicated.

a PCE of 1.11% and a  $V_{OC}$  of 0.97 V (Table 3). Notably, thermal annealing or the introduction of additives cannot clearly improve the performances of solar cells with **TADPP3** or **TADPP2-TT** after blending with either **PC<sub>61</sub>BM** or **PC<sub>71</sub>BM**.

Compound **TADPP3** was also investigated as an n-type photovoltaic material to construct solar cells after blending with **P3HT** in different weight ratios. For example, Figure 6 shows the respective  $J$ - $V$  curve and IPCE spectrum for the solar cell with **TADPP3** after blending with **P3HT** in a weight ratio of 1:2 after thermal annealing. As listed in Table 3, the  $V_{OC}$  of these OSCs with **TADPP3** and **P3HT** is remarkably high, up to 1.11 V. This can be attributed to the large energy difference (1.33 eV) between the HOMO of **P3HT** and the LUMO of **TADPP3**. The solar cell with **TADPP3** and **P3HT** in a weight ratio of 1:1 shows a PCE of 0.47%, which increases to 0.87% after thermal annealing of the active layer at 150 °C for 10 min. This is mainly owing to the increase in  $J_{SC}$  from 1.21 to 1.97  $\text{mA cm}^{-2}$ . The PCE is further enhanced to 1.08% by varying the weight ratio of **P3HT** and **TADPP3** to 2:1 after thermal annealing of the active layer at 150 °C. Similarly, optimization of the weight ratios and thin-film thicknesses was performed, but the enhancement of PCE was not observed. Also, post-treatments, including thermal annealing and the introduction of additives, did not lead to an increase in PCE.

As depicted in Figures 5 and 6, the blending of thin films of **TADPP3/PC<sub>71</sub>BM**, **TADPP2-TT/PC<sub>71</sub>BM**, and **P3HT/TADPP3** displayed broad IPCE spectra from  $\lambda \approx 300$  to 700 nm. These IPCE spectra correspond well to the respective UV/Vis absorption profiles (see Figures S5 and S6 in the Supporting Information); this indicates that absorbed

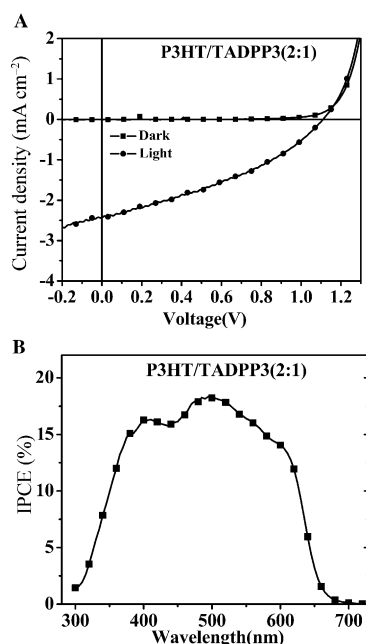


Figure 6. A)  $J$ - $V$  curves and B) IPCE spectra of OSCs with the respective blended thin films of **P3HT/TADPP3** after annealing at 150°C; the weight ratios are indicated.

photons contribute to the photovoltaic conversion. The maximum monochromatic IPCEs appear at  $\lambda \approx 500$  nm for OSCs with **TADPP3/PC<sub>71</sub>BM**, **TADPP2-TT/PC<sub>71</sub>BM**, and **P3HT/TADPP3**.

The blended thin films of **TADPP3** or **TADPP2-TT** with either **PC<sub>71</sub>BM** or **P3HT** were characterized with AFM and XRD techniques. Figure S7 in the Supporting Information shows AFM height and phase images of the blended films of **TADPP3** with **PC<sub>71</sub>BM** (1:2 in weight ratio) and **TADPP2-TT** with **PC<sub>71</sub>BM** (1:2 in weight ratio) without any post-treatments. The surface morphology of the thin film of **TADPP3** with **PC<sub>71</sub>BM** is more uniform than that with **TADPP2-TT** and **PC<sub>71</sub>BM**; thin films of **TADPP3** and **TADPP2-TT** with **PC<sub>71</sub>BM** exhibit root-mean-square (RMS) roughnesses of 0.97 and 1.49 nm, respectively. Moreover, no clear phase contrast was observed from the phase images for either thin film. Out-of-plane and in-plane XRD data reveal no strong peaks (see Figure S8 in the Supporting Information), and the weak, broad signal at around 19° may be due to the short intermolecular contacts of **PC<sub>71</sub>BM**. These results reveal that thin films of **TADPP3** and **TADPP2-TT** with **PC<sub>71</sub>BM** are amorphous and show low crystallinity. This is in agreement with the observation that OSCs with these thin films as active layers possess low  $J_{SC}$  and FF values (see Table 3).

Figure S9 in the Supporting Information shows AFM height and phase images of as-prepared and annealed **TADPP3/P3HT** films. Interpenetrating networks were observed in the AFM phase images. The height image of the as-prepared thin film comprises small domains of around  $90 \times 110$  nm<sup>2</sup> with a surface roughness of 3.06 nm. After thermal annealing at 150°C, there were significant changes in

the surface morphology. The domain sizes increased to about  $150 \times 200$  nm<sup>2</sup>, and the surface roughness reached 5.09 nm. This probably resulted from the self-organization of **P3HT** chains after thermal annealing. A strong peak at 4.5° and a weak signal at 23.6° were detected in the out-of-plane and in-plane XRD patterns (see Figure S10 in the Supporting Information) for a thin film of **TADPP3** with **P3HT** after annealing at 150°C. This may be due to the ordered packing of **P3HT** chains, which is beneficial for ordered structure formation and charge transport within the thin film.

## Conclusion

Two conjugated molecules, **TADPP3** and **TADPP2-TT**, were synthesized and investigated. Three and two D-A-D moieties that contained dithienyldiketopyrrolopyrrole were substituted at the *meta* positions of benzene in **TADPP3** and **TADPP2-TT**, respectively; **TADPP2-TT** also included one 2,2':5',2''-terthiophene moiety. The respective cyclic voltammetric and absorption spectra data revealed that **TADPP3** and **TADPP2-TT** possessed similar HOMO and LUMO energies of approximately -5.2 and -3.4 eV, respectively. This was consistent with DFT calculations, which indicated that the 2,2':5',2''-terthiophene moiety in **TADPP2-TT** made no contribution to either the HOMO or LUMO. Based on the transfer and output characteristics of OFETs, thin films of **TADPP3** and **TADPP2-TT** exhibited p-type semiconducting behavior with hole mobilities of  $2.36 \times 10^{-3}$  and  $3.76 \times 10^{-4}$  cm<sup>2</sup>V<sup>-1</sup>s<sup>-1</sup> after thermal annealing. Compound **TADPP3** could be utilized as both p- and n-type photovoltaic materials. A solar cell with a thin film of **TADPP3** with **PC<sub>71</sub>BM** in a weight ratio of 1:2 exhibited a high  $V_{OC}$  of 0.99 V and a PCE of 2.47%. The blended thin film of **TADPP3** with **P3HT** in a weight ratio of 1:2 yielded a high  $V_{OC}$  of 1.11 V and a PCE of 1.08% after thermal annealing. OSCs could be also fabricated with blended thin films of **TADPP2-TT** and **PC<sub>71</sub>BM**, and  $V_{OC}$  and PCE values reached 0.97 V and 1.11%, respectively, when the weight ratio of **TADPP2-TT** and **PC<sub>71</sub>BM** was 1:2. However, these OSCs with **TADPP3** and **TADPP2-TT** exhibited low  $J_{SC}$  and FF values; this could be attributed to low crystallinity and poor morphologies for blended thin films based on AFM and XRD studies. Further studies include optimization of molecular structures with such 3D-conjugated frameworks, which may enable to improve the thin-film morphology and crystallinity.

## Experimental Section

### Materials and Characterization Techniques

The reagents and starting materials employed were commercially available and used without any further purification, unless specified otherwise. Compound **5** was synthesized according to published procedures.<sup>[16c]</sup> <sup>1</sup>H and <sup>13</sup>C NMR spectra were recorded on a Bruker AVANCE III 400 MHz spectrometer. Elemental analysis was performed on a Carlo Erba

model 1160 elemental analyzer. MALDI-TOF MS were recorded with a BEFLEX III spectrometer. TGA measurements were carried out on a Shimadzu DTG-60 instrument under a flow of dry nitrogen, heated from room temperature to 550°C, with a heating rate of 10°Cmin<sup>-1</sup>. DSC (PerkinElmer 7 series thermal analyzers) measurements were performed under a nitrogen atmosphere at a heating rate of 10°Cmin<sup>-1</sup>. Absorption spectra were measured with a Jasco V-570 UV/Vis spectrophotometer. Cyclic voltammetric measurements were carried out in a conventional three-electrode cell by using Pt wires of 2.0 mm in diameter as working and counter electrodes and an Ag/AgCl reference electrode on a computer-controlled CHI660C instrument at room temperature. The GIXRD data were measured at 1W1A, Beijing Synchrotron Radiation Facility. AFM images of the thin films were obtained on a Nanoscope IIIa (Digital Instruments) microscope operating in tapping mode.

#### Synthesis of TADPPP3

Compound **5** (600 mg, 1.0 mmol), [Pd(PPh<sub>3</sub>)<sub>4</sub>] (23.1 mg, 0.02 mmol), and CuI (1.1 mg, 0.006 mmol) were loaded into a flame-dried, one-necked flask mounted with a condenser. Degassed/anhydrous toluene (20 mL) and (iPr)<sub>2</sub>NH (5 mL) were added, followed by the addition of 1,3,5-triethynylbenzene (30 mg, 0.2 mmol). The reaction mixture was then heated to 90°C and stirred overnight. After cooling to room temperature, water (25 mL) was added and the mixture was extracted with ethyl acetate (3 × 25 mL). The organic phase was dried over MgSO<sub>4</sub> and filtered. Then, the filtrate was concentrated under reduced pressure. The crude product was purified by flash chromatography with CH<sub>2</sub>Cl<sub>2</sub>/*n*-hexane (v/v, 1:2) as the eluent to afford TADPPP3 (248 mg, 72%). M.p. 210.5–211.7°C; <sup>1</sup>H NMR (400 MHz, CDCl<sub>3</sub>): δ = 8.95 (d, *J* = 4 Hz, 3H), 8.89 (d, *J* = 4 Hz, 3H), 7.70 (s, 3H), 7.66–7.65 (m, 3H), 7.42–7.41 (m, 3H), 7.29–7.26 (m, 3H), 4.07–4.02 (m, 12H), 1.89–1.88 (m, 6H), 1.42–1.26 (m, 48H), 0.94–0.89 ppm (m, 36H); <sup>13</sup>C NMR (100 MHz, CDCl<sub>3</sub>): δ = 161.8, 161.7, 141.1, 139.1, 135.9, 135.3, 134.2, 133.7, 131.5, 131.1, 129.9, 128.7, 127.3, 123.7, 109.1, 108.2, 95.3, 84.2, 46.2, 46.1, 39.3, 39.2, 30.4, 30.3, 29.8, 29.5, 28.4, 23.7, 23.2, 14.2, 10.6 ppm; MS (MALDI-TOF): *m/z*: 1717.7 [*M*+H]<sup>+</sup>; elemental analysis calcd (%) for C<sub>102</sub>H<sub>120</sub>N<sub>6</sub>O<sub>6</sub>S<sub>6</sub>: C 71.29, H 7.04, N 4.89, S 11.19; found: C 71.38, H 7.01, N 4.93, S 11.05.

#### Synthesis of Compound 6

*n*BuLi (1.6 M in hexane, 1.13 mL, 1.8 mmol) was added to a stirred solution of 1,3,5-triethynylbenzene (300 mg, 2 mmol) in THF (20 mL) at –78°C, and the resulting mixture was stirred at –78°C for 30 min. TIPSCl (3.4 mL, 23.9 mmol) was then added and the reaction mixture was stirred for another 30 min at –78°C. The reaction was quenched by the addition of a saturated aqueous solution of NH<sub>4</sub>Cl and extracted with Et<sub>2</sub>O. The organic layer was dried over Na<sub>2</sub>SO<sub>4</sub> and concentrated to afford **6** (470 mg, 85%). The product was used in the next step without further purification.

#### Synthesis of Compound 7

Compound **5** (600 mg, 1.0 mmol), [Pd(PPh<sub>3</sub>)<sub>4</sub>] (23.1 mg, 0.02 mmol), and CuI (0.95 mg, 0.005 mmol) were loaded into a flame-dried, one-necked flask mounted with a condenser. Degassed/anhydrous toluene (20 mL) and (iPr)<sub>2</sub>NH (5 mL) were added, followed by the addition of compound **6** (76.5 mg, 0.25 mmol). The reaction mixture was then heated to 90°C and stirred overnight. After cooling to room temperature, water (25 mL) was added and the mixture was extracted with ethyl acetate (3 × 25 mL). The organic phase was dried over MgSO<sub>4</sub> and filtered. Then, the filtrate was concentrated under reduced pressure. The crude product was purified by flash chromatography with CH<sub>2</sub>Cl<sub>2</sub>/*n*-hexane (v/v, 1:5) as the eluent to afford **7** (252 mg, 75%). <sup>1</sup>H NMR (400 MHz, CDCl<sub>3</sub>): δ = 8.95 (d, *J* = 4 Hz, 2H), 8.89 (d, *J* = 4 Hz, 2H), 7.65–7.63 (m, 5H), 7.41 (d, *J* = 4 Hz, 2H), 7.29 (d, *J* = 4 Hz, 2H), 4.05–4.00 (m, 8H), 1.89 (s, 4H), 1.41–1.33 (m, 32H), 1.12–1.09 (m, 21H), 0.93–0.84 ppm (m, 24H); <sup>13</sup>C NMR (100 MHz, CDCl<sub>3</sub>): δ = 161.2, 161.1, 140.5, 138.6, 135.3, 134.8, 134.4, 133.2, 133.0, 130.7, 130.5, 129.3, 128.1, 126.9, 124.2, 122.8, 107.6, 104.3, 95.0, 92.7, 83.2, 45.6, 45.5, 38.7, 38.6, 29.8, 29.7, 29.3, 27.90, 27.88, 23.1, 22.61, 13.59, 13.57, 10.8, 10.03, 10.02 ppm; MS (MALDI-TOF): *m/z*:

1351.7 [*M*+H]<sup>+</sup>; elemental analysis calcd (%) for C<sub>81</sub>H<sub>102</sub>N<sub>4</sub>O<sub>4</sub>S<sub>4</sub>Si: C 71.96, H 7.06, N 4.41, S 9.48; found: C 71.88, H 7.11, N 4.52, S 9.39.

#### Synthesis of TADPP2-TT

K<sub>2</sub>CO<sub>3</sub> (21.8 mg, 0.16 mmol) was added to a stirred solution of compound **7** (216 mg, 0.16 mmol) in THF (40 mL) at 25°C, and the reaction mixture was stirred for 30 min. Then, 5-bromo-2,2':5',2''-terthiophene (103 mg, 0.32 mmol), [Pd(PPh<sub>3</sub>)<sub>4</sub>] (9 mg, 0.008 mmol), CuI (0.4 mg, 0.002 mmol), and (iPr)<sub>2</sub>NH (5.0 mL) were added to the solution. The mixture was heated to reflux and stirred overnight. After cooling to room temperature, water (25 mL) was added and the mixture was extracted with ethyl acetate (3 × 25 mL). The organic phase was dried over MgSO<sub>4</sub> and filtered, and the filtrate was concentrated under reduced pressure. The crude product was purified by flash chromatography with CH<sub>2</sub>Cl<sub>2</sub>/*n*-hexane (v/v, 1:2) as the eluent to afford TADPP2-TT (152 mg, 67%). M.p. 96.5–98.9°C; <sup>1</sup>H NMR (400 MHz, CD<sub>2</sub>Cl<sub>2</sub>): δ = 8.83 (d, *J* = 4 Hz, 2H), 8.78 (d, *J* = 4 Hz, 2H), 7.62–7.59 (m, 5H), 7.38–7.37 (m, 2H), 7.22–7.17 (m, 4H), 7.14–7.13 (m, 1H), 7.07–7.02 (m, 3H), 6.97–6.95 (m, 1H), 3.95–3.92 (m, 8H), 1.80–1.77 (m, 4H), 1.30–1.16 (m, 32H), 0.85–0.76 ppm (m, 24H); <sup>13</sup>C NMR (100 MHz, CD<sub>2</sub>Cl<sub>2</sub>): δ = 161.5, 161.4, 140.7, 138.9, 135.3, 134.9, 133.2, 131.5, 131.3, 131.0, 129.9, 128.3, 127.5, 122.8, 108.9, 108.1, 96.7, 84.6, 45.8, 45.7, 39.2, 39.1, 30.1, 30.0, 29.7, 28.35, 28.32, 23.5, 23.0, 13.8, 10.2 ppm; MS (MALDI-TOF): *m/z*: 1441.9 [*M*+H]<sup>+</sup>; elemental analysis calcd (%) for C<sub>84</sub>H<sub>88</sub>N<sub>4</sub>O<sub>4</sub>S<sub>7</sub>: C 69.96, H 6.15, N 3.89, S 15.56; found: C 69.74, H 5.89, N 3.65, S 15.37.

## Acknowledgements

This research was financially supported by the Chinese Academy of Sciences, NSFC (no.51373181) and the State Key Basic Research Program. We thank Prof. Yongfang Li for helpful discussions and permission to use the facility for fabrication of OSCs. We also gratefully acknowledge the assistance of scientists of the Diffuse X-ray Scattering Station at Beijing Synchrotron Radiation Facility for measuring the GIXRD data.

- [1] W. K. Chan, Y. Chen, Z. Peng, L. P. Yu, *J. Am. Chem. Soc.* **1993**, *115*, 11735–11743.
- [2] a) S. Qu, H. Tian, *Chem. Commun.* **2012**, *48*, 3039–3051; b) C. B. Nielsen, M. Turbiez, I. McCulloch, *Adv. Mater.* **2013**, *25*, 1859–1880.
- [3] a) Y. N. Li, P. Sonar, L. Murphy, W. Hong, *Energy Environ. Sci.* **2013**, *6*, 1684–1710; b) M. A. Naik, S. Patil, *J. Polym. Sci. Part A* **2013**, *51*, 4241–4260.
- [4] a) H. Chen, Y. Guo, G. Yu, Y. Zhao, J. Zhang, D. Gao, H. Liu, Y. Q. Liu, *Adv. Mater.* **2012**, *24*, 4618–4622; b) Y. Zhao, Y. L. Guo, Y. Q. Liu, *Adv. Mater.* **2013**, *25*, 5372–5391; c) Z. X. Cai, H. W. Luo, X. Chen, G. X. Zhang, Z. T. Liu, D. Q. Zhang, *Chem. Asian J.* **2014**, *9*, 1068–1075.
- [5] a) O. P. Lee, A. T. Yiu, P. M. Beaujuge, C. H. Woo, T. W. Holcombe, J. E. Millstone, J. D. Douglas, M. S. Chen, J. M. J. Fréchet, *Adv. Mater.* **2011**, *23*, 5359–5363; b) L. Li, Y. Huang, J. Peng, Y. Cao, X. B. Peng, *J. Mater. Chem. A* **2013**, *1*, 2144–2150; c) S. L. Zhang, B. Jiang, C. L. Zhan, J. H. Huang, X. Zhang, H. Jia, A. L. Tang, L. L. Chen, J. N. Yao, *Chem. Asian J.* **2013**, *8*, 2407–2416.
- [6] a) H. Tan, X. Deng, J. Yu, B. Zhao, Y. Wang, Y. Liu, W. Zhu, H. Wu, Y. Cao, *Macromolecules* **2013**, *46*, 113–118; b) S. Zhang, L. Ye, Q. Wang, Z. Li, X. Guo, L. Huo, H. Fan, J. H. Hou, *J. Phys. Chem. C* **2013**, *117*, 9550–9557.
- [7] a) J. C. Bijleveld, A. P. Zoombelt, S. G. J. Mathijssen, M. M. Wienk, M. Turbiez, D. M. de Leeuw, R. A. J. Janssen, *J. Am. Chem. Soc.* **2009**, *131*, 16616–16617; b) W. Li, W. S. C. Roelofs, M. M. Wienk, R. A. J. Janssen, *J. Am. Chem. Soc.* **2012**, *134*, 13787–13795; c) W. Li, K. H. Hendriks, A. Furlan, W. S. C. Roelofs, M. M. Wienk, R. A. J. Janssen, *J. Am. Chem. Soc.* **2013**, *135*, 18942–18948.
- [8] a) L. Huo, J. Hou, H.-Y. Chen, S. Zhang, Y. Jiang, T. L. Chen, Y. Yang, *Macromolecules* **2009**, *42*, 6564–6571; b) L. Dou, J. Gao, E.

- Richard, J. You, C. C. Chen, K. C. Cha, Y. He, G. Li, Y. Yang, *J. Am. Chem. Soc.* **2012**, *134*, 10071–10079.
- [9] a) V. Coropceanu, J. Cornil, D. A. Filho, Y. Olivier, R. Silbey, J. L. Brédas, *Chem. Rev.* **2007**, *107*, 926–952; b) B. Walker, C. Kim, T. Q. Nguyen, *Chem. Mater.* **2011**, *23*, 470–482; c) Y. Lin, Y. Li, X. W. Zhan, *Chem. Soc. Rev.* **2012**, *41*, 4245–4272; d) Y. F. Li, *Acc. Chem. Res.* **2012**, *45*, 723–733; e) L. Dou, J. You, Z. Hong, Z. Xu, G. Li, R. A. Street, Y. Yang, *Adv. Mater.* **2013**, *25*, 6642–6671; f) Z. He, H. Wu, Y. Cao, *Adv. Mater.* **2014**, *26*, 1006–1024.
- [10] H. U. Habermeier, *Mater. Today* **2007**, *10*, 34–43.
- [11] a) F. S. Kim, X. Guo, M. D. Watson, S. A. Jenekhe, *Adv. Mater.* **2010**, *22*, 478–482; b) Y. Sun, S. C. Chien, H. L. Yip, Y. Zhang, K. S. Chen, D. F. Zeigler, F. C. Chen, B. Lin, A. K. Y. Jen, *J. Mater. Chem.* **2011**, *21*, 13247; c) M. S. Chen, J. R. Niskala, D. A. Unruh, C. K. Chu, O. P. Lee, J. M. J. Fréchet, *Chem. Mater.* **2013**, *25*, 4088–4096.
- [12] a) V. Steinmann, N. M. Kronenberg, M. R. Lenze, S. M. Graf, D. Hertel, K. Meerholz, H. Bürckstümmer, E. V. Tulyakova, F. Würthner, *Adv. Energy Mater.* **2011**, *1*, 888–893; b) Q. Liu, H. Zhan, C. L. Ho, F. R. Dai, Y. Fu, Z. Xie, W. Y. Wong, *Chem. Asian J.* **2013**, *8*, 1892–1900.
- [13] a) H. Bürckstümmer, E. V. Tulyakova, M. Deppisch, M. R. Lenze, N. M. Kronenberg, M. Gsanger, M. Stolte, K. Meerholz, F. Würthner, *Angew. Chem.* **2011**, *123*, 11832–11836; *Angew. Chem. Int. Ed.* **2011**, *50*, 11628–11632; b) Y. Sun, G. C. Welch, W. L. Leong, C. J. Takacs, G. C. Bazan, A. J. Heeger, *Nat. Mater.* **2012**, *11*, 44–48.
- [14] a) P. L. T. Boudreault, J. W. Hennek, S. Loser, R. P. Ortiz, B. J. Eckstein, A. Facchetti, T. J. Marks, *Chem. Mater.* **2012**, *24*, 2929–2942; b) S. Loser, H. Miyachi, J. W. Hennek, J. Smith, C. Huang, A. Facchetti, T. J. Marks, *Chem. Commun.* **2012**, *48*, 8511–8513.
- [15] a) L. Ye, S. Zhang, W. Ma, B. Fan, X. Guo, Y. Huang, H. Ade, J. H. Hou, *Adv. Mater.* **2012**, *24*, 6335–6341; b) X. Zhang, Z. Lu, L. Ye, C. Zhan, J. Hou, S. Zhang, B. Jiang, Y. Zhao, J. Huang, S. Zhang, Y. Liu, Q. Shi, Y. Q. Liu, J. N. Yao, *Adv. Mater.* **2013**, *25*, 5791–5797; c) R. Shivanna, S. Shoaee, S. Dimitrov, S. K. Kandappa, S. Rajaram, J. R. Durrant, K. S. Narayan, *Energy Environ. Sci.* **2014**, *7*, 435–441.
- [16] a) S. Roquet, A. Cravino, P. Leriche, O. Aleque, P. Frevemes, J. Roncali, *J. Am. Chem. Soc.* **2006**, *128*, 3459–3466; b) B. Walker, A. B. Tamayo, X. D. Dang, P. Zalar, J. H. Seo, A. Garcia, M. Tantiwiwat, T. Q. Nguyen, *Adv. Funct. Mater.* **2009**, *19*, 3063–3069; c) S. Loser, C. J. Bruns, H. Miyachi, R. P. Ortiz, A. Facchetti, S. I. Stupp, T. J. Marks, *J. Am. Chem. Soc.* **2011**, *133*, 8142–8145; d) Y. H. Chen, L. Y. Lin, C. W. Lu, F. Lin, Z. Y. Huang, H. W. Lin, P. H. Wang, Y. H. Liu, K. T. Wong, J. Wen, D. J. Miller, S. B. Darling, *J. Am. Chem. Soc.* **2012**, *134*, 13616–13623; e) J. Huang, C. L. Zhan, X. Zhang, Y. Zhao, Z. Lu, H. Jia, B. Jiang, J. Ye, S. Zhang, A. Tang, Y. Q. Liu, Q. B. Pei, J. N. Yao, *ACS Appl. Mater. Interfaces* **2013**, *5*, 2033–2039; f) L. Y. Lin, Y. H. Chen, Z. Y. Huang, H. W. Lin, S. H. Chou, F. Lin, C. W. Chen, Y. H. Liu, K. T. Wong, *J. Am. Chem. Soc.* **2011**, *133*, 15822–15825.
- [17] a) R. Fitzner, E. Osteritz, A. Mishra, G. Schulz, E. Reinold, M. Weil, C. Körner, H. Ziehlke, C. Elschner, K. Leo, M. Riede, M. Pfeiffer, C. Urich, P. Bäuerle, *J. Am. Chem. Soc.* **2012**, *134*, 11064–11067; b) M. Weideler, C. D. Wessendorf, J. Hanisch, E. Ahlsweide, G. Gotz, M. Linden, G. Schulz, E. M. Osteritz, A. Mishra, P. Bäuerle, *Chem. Commun.* **2013**, *49*, 10865–10867.
- [18] a) Z. M. Tang, T. Lei, K. J. Jiang, Y. L. Song, J. Pei, *Chem. Asian J.* **2010**, *5*, 1911–1917; b) E. Ripaud, T. Rousseau, P. Leriche, J. Roncali, *Adv. Energy Mater.* **2011**, *1*, 540–545; c) Y. Lin, P. Cheng, Y. Li, X. W. Zhan, *Chem. Commun.* **2012**, *48*, 4773–4775; d) Y. S. Chen, X. J. Wan, G. K. Long, *Acc. Chem. Res.* **2013**, *46*, 2645–2655; e) W. Jiang, L. Ye, X. Li, C. Xiao, F. Tan, W. Zhao, J. Hou, Z. Wang, *Chem. Commun.* **2014**, *50*, 1024–1026.
- [19] a) R. M. Adhikari, L. Duan, L. Hou, Y. Qiu, D. C. Neckers, B. K. Shah, *Chem. Mater.* **2009**, *21*, 4638–4644; b) J. L. Wang, Z. He, H. Wu, H. Cui, Y. Li, Q. Gong, Y. Cao, J. Pei, *Chem. Asian J.* **2010**, *5*, 1455–1465; c) M. Seri, A. Marrocchi, D. Bagnis, R. Ponce, A. Taticchi, T. J. Marks, A. Facchetti, *Adv. Mater.* **2011**, *23*, 3827–3831; d) A. Tang, L. Li, Z. Lu, J. Huang, H. Jia, C. L. Zhan, Z. A. Tan, Y. F. Li, J. N. Yao, *J. Mater. Chem. A* **2013**, *1*, 5747–5757.
- [20] a) C. J. Brabec, C. Winder, N. S. Sariciftci, J. C. Hummelen, A. Dhannabalan, P. A. Hal, R. A. J. Janssen, *Adv. Funct. Mater.* **2002**, *12*, 709–712; b) H. Shang, H. Fan, Y. Liu, W. Hu, Y. F. Li, X. W. Zhan, *Adv. Mater.* **2011**, *23*, 1554–1557; c) J. Zhou, X. Wan, Y. Liu, Y. Zuo, Z. Li, G. He, G. Long, W. Ni, C. Li, X. Su, Y. S. Chen, *J. Am. Chem. Soc.* **2012**, *134*, 16345–16351; d) J. Zhou, Y. Zuo, X. Wan, G. Long, Q. Zhang, W. Ni, Y. Liu, Z. Li, G. He, C. Li, B. Kan, M. Li, Y. S. Chen, *J. Am. Chem. Soc.* **2013**, *135*, 8484–8487.
- [21] Y. Ie, T. Sakurai, S. Jinnai, M. Karakawa, K. Okuda, S. Mori, Y. Aso, *Chem. Commun.* **2013**, *49*, 8386–8388.

Received: January 19, 2014

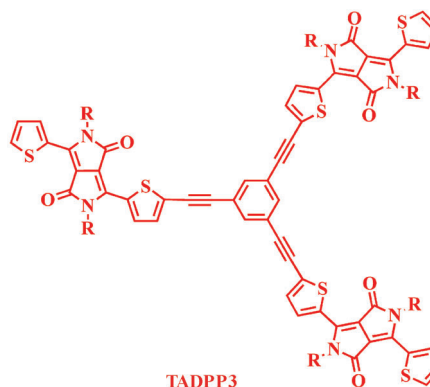
Published online: ■ ■ ■, 0000

# FULL PAPER

## Solar Cells

Chenmin Yu, Chang He, Yang Yang,  
Zhengxu Cai, Hwei Luo,  
Wenqiang Li, Qian Peng,  
Guanxin Zhang, Zitong Liu,\*  
Deqing Zhang\* ————— ■■■■-■■■■

 **New Conjugated Molecules with Two and Three Dithienyldiketopyrrolopyrrole (DPP) Moieties Substituted at *meta* Positions of Benzene toward p- and n-Type Organic Photovoltaic Materials**



**Star-shaped small molecules:** Two conjugated molecules, **TADPP3** and **TADPP2-TT**, have been developed and applied in solution-processed organic solar cells. Molecule **TADPP3**

can be applied as both a donor and an acceptor. The resulting solar cells have a high open-circuit voltage (>0.9 V) and the power conversion efficiency reaches 2.47%.